Materials Today Bio 12 (2021) 100167

Contents lists available at ScienceDirect

Materials Today Bio

journal homepage: www.journals.elsevier.com/materials-today-bio

Dual-targeted carbon-dot-drugs nanoassemblies for modulating Alzheimer's related amyloid-β aggregation and inhibiting fungal infection

Chaoren Yan [a,1], Chaoli Wang [b,1], Xu Shao [a], Qi Shu [a], Xiaoling Hu [a,*], Ping Guan [a,**], Yonggang Teng [c], Yuan Cheng [d,e,***]

[a] Department of Chemistry, School of Chemistry and Chemical Engineering, Northwestern Polytechnical University, Xi'an, 710072, PR China
[b] Department of Pharmaceutical Analysis, School of Pharmacy, Air Force Medical University, Xi'an, 710032, PR China
[c] Department of Thoracic Surgery, The Second Affiliated Hospital of Air Force Medical University, Xi'an, China
[d] Monash Suzhou Research Institute, Suzhou, 215123, PR China
[e] Department of Mechanical and Aerospace Engineering, Monash University, Clayton Victoria, 3800, Melbourne, Australia

ARTICLE INFO

Keywords:
Glycosylated carbon dots
Epigallocatechin-3-gallate
Amyloid-βpeptide
Candida albicans
Alzheimer's disease

ABSTRACT

Amyloid aggregation and fungal infection, especially amyloid beta (Aβ) peptide and *Candida albicans* are considered as two of the crucial pathogenic agents in Alzheimer's disease (AD). In this work, we propose an innovative treatment strategy for AD, targeting at not only Aβ aggregation but also *Candida albicans* infection. Here, a high-performance nanomaterial, namely gCDs-E, have been prepared by self-assembled of glycosylated carbon dots (gCDs) and epigallocatechin-3-gallate (EGCG). Surprisingly, gCDs-E can not only suppress the fibrillation of Aβ and disaggregate Aβ fibrils, but also effectively inhibit the activity of *Candida albicans*. More importantly, the prepared gCDs-E can effectively cut down the cytotoxicity of amyloid aggregations, and the cell viability reached to 99.2%. In addition, the capability of the gCDs-E for blood brain barrier (BBB) penetration was also observed using a normal mice model. Above all, the gCDs-E greatly cleaned Aβ deposition and improved memory impairment in APP/PS1 transgenic AD model mice, confirming its potential as therapeutic agent for AD treatment.

1. Introduction

Alzheimer's disease (AD), also namely dementia, is the most prevalent form of neurodegenerative disorder [1–3]. Although the pathogenesis of AD has not been clearly and thoroughly confirmed, its emphatic pathological traits have been verified, which is the extracellular deposits of amyloid aggregation from the amyloid-β peptides (Aβ) [4–10]. The therapeutic and preventive methods of AD including inhibiting the aggregation of Aβ into fibrils and oligomers is also effectual and widely accepted [11–17]. However, the recent failure of clinical trials suggests that further efforts on AD research is still demanding [12]. Interestingly, recent intense research indicates that some pathogenic microorganisms exist in the brain and postulated to be involved with Aβ or even to AD [18–22]. For example, Pisa et al. [18] directly visualized fungal components inside neurons from AD patients. Wu et al.' [20] showed that *Candida albicans* can cross the BBB and cause a highly localized cerebritis. Moreover, Aβ accumulates within the activated microglial and astroglia cells, which are induced by *Candida albicans*. These evidences even indicated that Aβ peptides enhanced both phagocytic and antifungal activity from cells. According to Wu's research [20], *Candida albicans* can cause a highly localized cerebritis marked by the accumulation of activated microglial and astroglial cells around yeast aggregates, forming fungal-induced glial granulomas. In addition, they found that large amounts of Aβ peptides and insoluble Aβ aggregation accumulated around the yeast cells. This related research indicates that the more serious the fungal infection, the more obvious amyloid fibrillation.

Currently, most of Aβ inhibitors including biomolecules [23–26], functionalized nanomaterials and nanoparticles [16,17,27–31], have been shown to decelerate the aggregation of Aβ and suppress cellular toxicity of amyloid. For example, Sun et al. [32] reported a mesoporous

* Corresponding author.
** Corresponding author.
*** Corresponding author. Monash Suzhou Research Institute, Suzhou, 215123, PR China.
E-mail addresses: huxl@nwpu.edu.cn (X. Hu), guanping1113@nwpu.edu.cn (P. Guan), yuan.cheng@monash.edu (Y. Cheng).
[1] Co-first author: Chaoren Yan; Chaoli Wang.

https://doi.org/10.1016/j.mtbio.2021.100167
Received 17 September 2021; Received in revised form 15 November 2021; Accepted 23 November 2021
Available online 27 November 2021

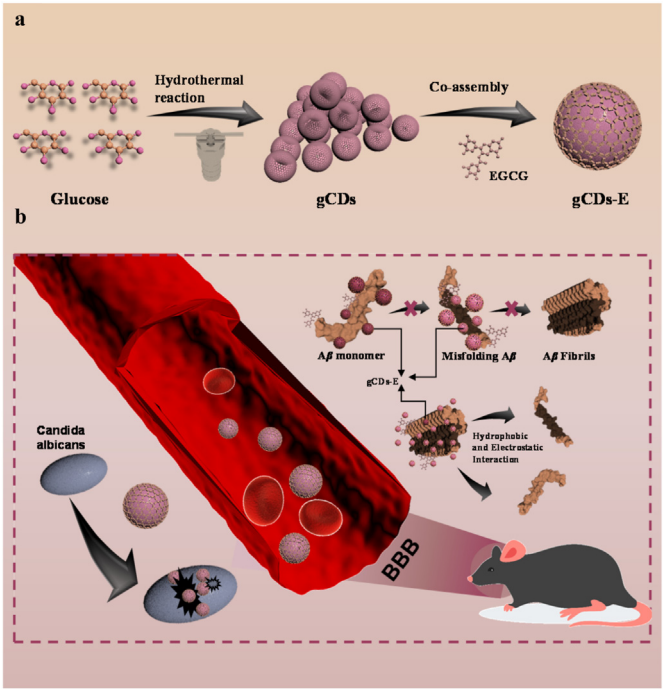

Scheme 1. (a) The preparation process of gCDs and gCDs-E. (b) Schematic illustration of the mechanism of gCDs-E for crossing BBB, suppressing Aβ aggregation and inhibiting *Candida albicans*.

nano-selenium release delivery system (MSe-Res/Fc-β-CD/Bor), and this nano-selenium release delivery system could inhibit aggregation of Aβ and improve memory impairment in APP/PS1 mice. In addition, Yang et al. [13] devised a novel nanochaperone based on mixed-shell polymeric micelle, and applied nanochaperone to selectively capture Aβ peptides, inhibit Aβ aggregation, and suppress Aβ-mediated cytotoxicity. Epigallocatechin-3-gallate (EGCG), the major components of green tea extract, exhibits effects of anti-inflammation, antifungals and modulation of β-amyloid self-assembly [26,28,33–38]. For example, previous studies have shown that EGCG enable to inhibit the growth of *Candida albicans*, and bind with unfolded Aβ for inhibiting the formation of β-sheet structure amyloid [26,28,35,36]. Moreover, the related research reveal that EGCG have not obvious cytotoxicity to HEK 293 cells after 24 h at 160 μg/mL EGCG, and caused 90% growth inhibition of tested strains of *C. albicans* [36,39]. Nevertheless, BBB is the major obstacles in the treatment of AD [11,40–42], while it's difficult for EGCG to overcome it spontaneously [21]. Considering the hampering effect of the BBB, designed nanocarriers with the ability to anchor EGCG and overcome the BBB are required. Fortunately, carbon dots (CDs) have greatly attracted our attention due to their ability of crossing the BBB, unique optical property and low toxicity [43–47]. For example, Xiao and Wang et al. demonstrated that GQDs enable to cross the BBB, inhibit aggregation of Aβ and rescue the cytotoxicity of Aβ oligomers [27,48]. Liyanage et al. also reported the capability of carbon nitride dots to penetrate the BBB [49]. Moreover, Leblanc's group deeply explored the mechanism of overcoming the BBB with CDs and verified the ability of CDs for inhibiting the human amyloid precursor protein and Aβ [50–53].

In this work, we propose a breakthrough strategy to consider these two possible pathogenic factors with unprecedented efficiency on inhibiting AD. A novel nanomaterial (gCDs-E) assembled from glycosylated carbon dots (gCDs) and EGCG (Scheme 1a) were fabricated, and its capability for treatment AD was explored. Different from traditional treatment strategies, Aβ aggregation and *Candida albicans* infection were both considered as possible pathogenic factors (Scheme 1b): Firstly, gCDs-E can effectively prevent misfolding of Aβ and inhibit its aggregation *in vitro*, and can remarkably reduce Aβ-mediated cytotoxicity. Next, gCDs-E can suppress the viability of *Candida albicans*, which preventing memory loss caused by fungal infection. Results from *in vitro* and *in vivo* experiments confirms the gCDs-E's high biocompatibility and ability of BBB penetration. Furthermore, gCDs-E can greatly clean Aβ deposition and improved memory impairment in APP/PS1 transgenic AD model mice.

2. Results and discussion

2.1. Characterization of gCDs and gCDs-E

Glycosylated carbon dots (gCDs) were firstly prepared using glucose as precursor by a solvothermal method. Following, gCDs-E was assembled from EGCG and gCDs through hydrogen bonding, π–π stacking interaction and electrostatic binding [54]. The morphology and particle size of gCDs and gCDs-E were characterized by transmission electron microscopy (TEM) and atomic force microscopy (AFM). As shown in Fig. 1a, gCDs exhibit a uniform dispersion without any apparent aggregation, and the average size is about 4.25 nm. AFM image (Fig. S1) reveals that gCDs disperse nicely with a particle's height about 1.5 nm. The size distribution of both TEM and AFM indicate that gCDs are discoidal shape. The corresponding high-resolution TEM (HRTEM) image (Fig. 1b) shows the obvious lattices in carbon cores of gCDs, and the distribution of lattice spacing is about 0.21 nm. The lattice spacing value correspond to the (100) inter-planar spacing, demonstrating the almost defect-free graphene crystalline structure [55–57]. Raman spectrum of gCDs (Fig. S2) shows that the intensity ratio (I_D/I_G) of characteristic D and G bands is about 0.71, and are positioned at 1335 and 1583 cm^{-1}, respectively. The ratio indicates that gCDs are consist of graphene structure (predominantly) and other disorder structure [57,58]. In the ^1H NMR spectra of gCDs, the peak at 9.53 ppm in Fig. S3 is the chemical shift of the carboxyl protons [56]. In addition, signals from the aromatic rings were detected at 8.37 ppm, which was attributed to graphitized cores' proton resonances [59]. Furthermore, the chemical shift values of aliphatic carbons are present in range from 1 to 5 ppm, which indicated the formation of glycosylated gCDs. As shown in Fig. 1c, it can be seen that the morphology of the prepared gCDs-E is circular or oval nanoparticle with a particles size about 25.5 nm. UV–Vis spectrum of gCDs is shown in Fig. 1d, the two obvious absorption peaks at 216 and 285 nm are attributed to the $\pi = \pi^*$ transition of C═C bond, and the weak absorption band in the range of 300–380 nm belongs to n-p* transition of the carboxylic C═O bond on the surface of gCDs [60,61]. The difference of UV–Vis spectrum (Fig. S4) for EGCG, gCDs and gCDs-E at 250–320 nm indicates that EGCG have been successfully anchored on the surface of gCDs. FL excitation and emission spectrum of gCDs (Fig. 1d) exhibits distinct and well-defined peaks at 362 and 445 nm. Fig. 1e and f represents the PL emission of the gCDs and gCDs-E solution under different excitation wavelengths. The gCDs (Fig. 1e) shows two stable emission centers at 445 and 545 nm. However, the as-prepared gCDs-E solution (Fig. 1f) exhibits distinctive excitation-dependent PL features, which can be attributed to the molecular interaction between EGCG and gCDs, and resulting in red shift of the emission [62]. In addition, after modification with EGCG, the formation of surface emissive traps as well as the varying size distribution of the gCDs caused by EGCG also lead to the wavelength-dependent fluorescence emission property [63,64]. The photoluminescence quantum yield (PLQY) of the gCDs and gCDs-E were calculated to be 12.7% and 9.8%, using the Quantaurus-QY equipment (Fig. S5). The full XPS spectrum presented in Fig. 1g and h shows two peaks at 284.8 and 532.2 eV, suggesting that the gCDs and gCDs-E consisted of C and O elements, and the calculated atomic ratios of gCDs and gCDs-E were 57.88%: 42.12% and 44.87%: 55.13%, respectively. In Fig. 1h and k, the high-resolution XPS spectrum of the C 1s band was separated into four peaks at 284.8, 285.8, 286.6, and 288.7 eV, which are assigned to C–C/C═C, C–O, C═O, and COOH, respectively. The O1s band (Fig. 1i and l) exhibits two peaks at 532.0 and 532.8 eV, respectively, which correspond to C═O and C–O groups. Then, Fourier

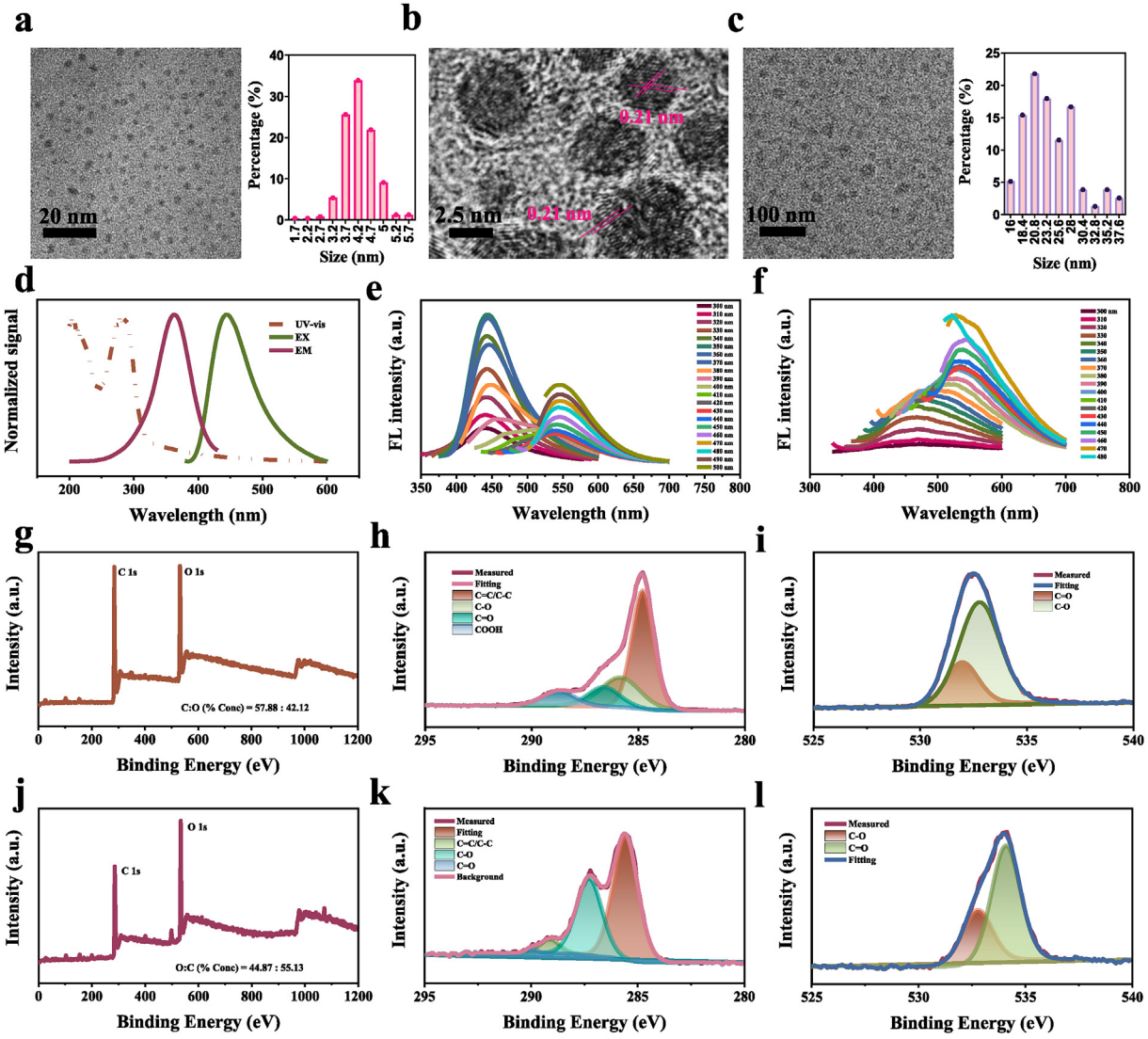

Fig. 1. (a) TEM image and the corresponding size distribution histogram of gCDs. (b) HR-TEM image of gCDs. (c) TEM image and the corresponding size distribution histogram of gCDs-E. (d) UV/Vis absorption spectrum of gCDs in water; the normalized FL emission and excitation spectra of gCDs in water. Fluorescence spectra of (e) gCDs and (f) gCDs-E solution at different excitation wavelengths. (g–i) XPS survey spectrum, high-resolution C 1s, and high-resolution O 1s spectrum of gCDs. (j–l) XPS survey spectrum, high-resolution C 1s, and high-resolution O 1s spectrum of gCDs-E.

transform infrared (FT-IR) was constructed to characterize the functional groups of gCDs and gCDs-E (Fig. S6). In the curve of gCDs (red line) and gCDs-E (purple line), absorption bands at 1642 cm^{-1}, 1108 cm^{-1} are corresponding to the stretching vibration of C═O and C–O [47,61], respectively. Therefore, hydroxyl and carboxyl are the main functional groups on the surface of gCDs and gCDs-E.

2.2. Inhibition and disaggregation of Aβ by gCDs and gCDs-E

Following, we investigated the potential role of the gCDs and gCDs-E in inhibiting Aβ fibrillization and disaggregating fibrils. TEM results are presented in Fig. 2a and Fig. S7. In the absence of gCDs or gCDs-E, mature $A\beta_{42}$ and $A\beta_{40}$ fibrils are obviously observed (Control group, Fig. 2a and Fig. S7a). The same assessments show that the gCDs-E (Fig. 2a and Fig. S7a) can predominantly disaggregate $A\beta_{42}$ and $A\beta_{40}$ fibrils into short fragments, with the average length of the fragments shortening from to 61 nm and 122 nm after gCDs-E treatment for 24 h, respectively. Corresponding DLS (Fig. S7b and Fig. S8) results also demonstrate the disaggregation ability of gCDs-E. In addition, the fibrillation process of $A\beta_{42}$ monomers incubated with gCDs or gCDs-E is also effectively suppressed (Fig. 2b), and the average length of the fragments is shorted from 648 nm to 3.6 nm after gCDs-E treatment for 24 h (Fig. 2d). Obviously, more significant disaggregation and inhibition performance of gCDs-E is also exhibited compared with gCDs (Fig. 2c and d). Furthermore, circular dichroism (CD) spectra were used to analyze the change of the secondary structure of Aβ peptides. The non-treated $A\beta_{42}$ monomers show random structures at 0 h and 30 min (Fig. 2e). However, the typical β-sheet structure of $A\beta_{42}$ occur from 6 h to 24 h in PBS solution (pH = 7.4), with positive and negative signals at 197 and 218 nm, respectively. Interestingly, the revealed β-sheet structure of $A\beta_{42}$ treated with the gCDs was significantly inhibited compared with control group (Fig. 2f). Moreover, gCDs-E treated $A\beta_{42}$ did not show β-sheet structures after 24 h, with only negative signals at 201 nm (Fig. 2f). Corresponding the fractional secondary structures were also analyzed using the algorithm CDNN (Fig. 2g). After treated with gCDs for 24 h, the β-sheet component of $A\beta_{42}$ decrease from 55.7% to 45.6% and the random coil components increase from 19.3% to 32.3%. The gCDs-E treated $A\beta_{42}$ shows a drop of β-sheet component from 55.7% to 31.2% and an increase of the random coil components from 19.3% to 35.9%. Furthermore, gCDs and gCDs-E can reverse the secondary structure of $A\beta_{42}$ fibrils. As shown

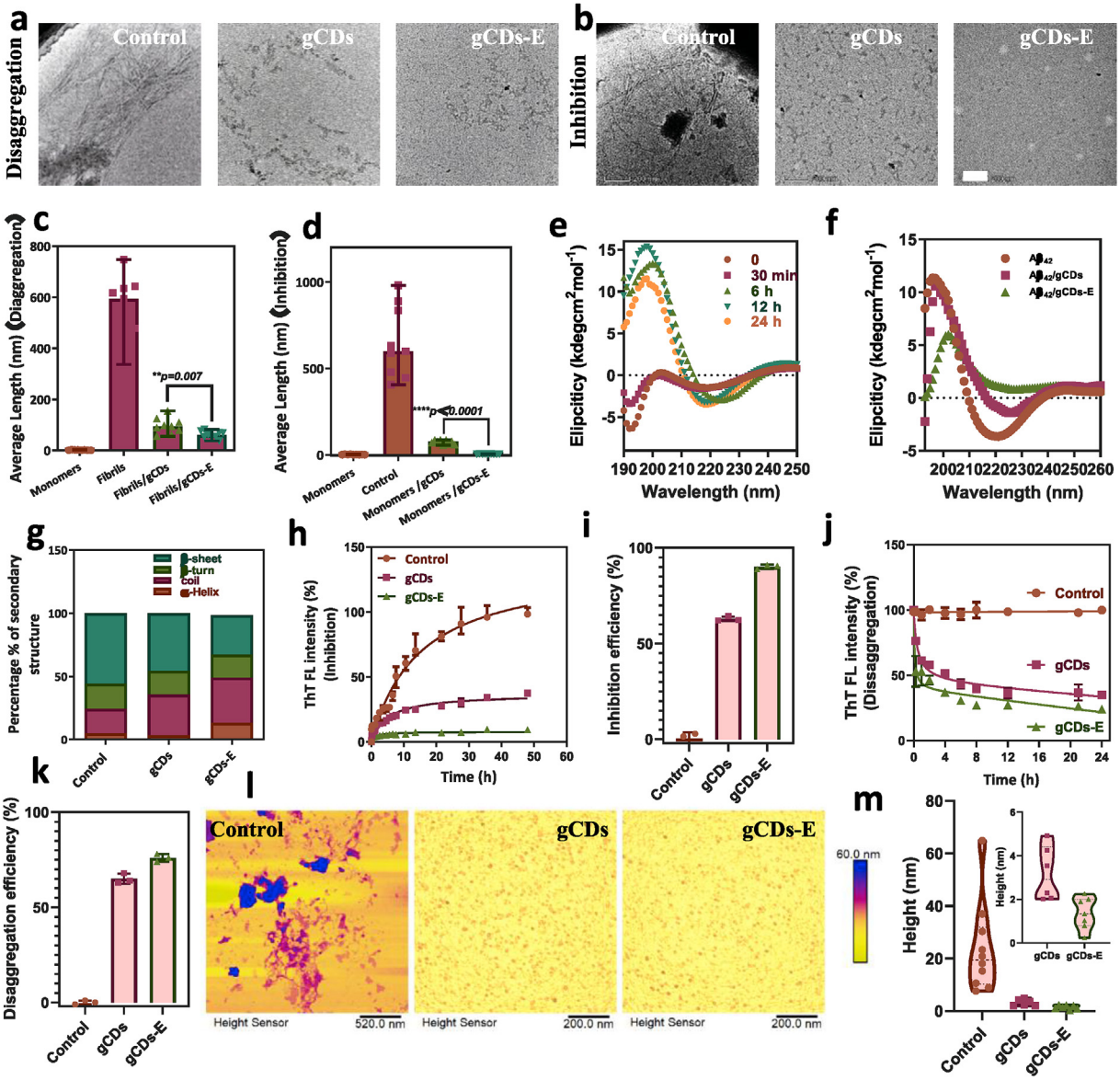

Fig. 2. (a–b) TEM images of Aβ_{42} fibrils or Aβ_{42} monomers (25 μM) incubated in the absence and presence of nanomaterials (gCDs or gCDs-E) after 24 h. (c–d) The corresponding size distribution histogram of TEM results. (e) CD spectra for misfolding process of Aβ_{42} monomers. (f) CD spectra for Aβ_{42} incubated in the absence and presence of gCDs or gCDs-E after 24 h. (g) The corresponding Fractional secondary structure contents ratio of Aβ_{42}. (h) ThT fluorescence assay of Aβ_{42} (25 μM), Aβ_{42}/gCDs and Aβ_{42}/gCDs-E in 48 h. (i) The corresponding inhibition efficiency of gCDs or gCDs-E. (j) ThT fluorescence assay of preformed Aβ fibrillar samples that were incubated with or without nanomaterials. (k) The corresponding disaggregation efficiency of gCDs or gCDs-E. (l) AFM images of Aβ_{42} monomers incubated with or without nanomaterials at pH 7.4 after 24 h. (m) Particle height distributions determined from AFM images, displayed as violin plots.

in Figs. S9a and b, the most negative peaks of Aβ_{42} fibrils is typical β-sheet structure at 0 h. After adding gCDs and gCDs-E, the negative peaks of Aβ_{42} fibrils were significantly reduced and the gCDs-E treated group became more significant than that of gCDs (Fig. S9b). Fig. 2h displays a series of inhibition curves of Aβ_{42} aggregation *in vitro* by a thioflavin T (ThT) assay. The fluorescence intensity of non-treated Aβ_{42} is sharply changed and much strong at 24 h due to the larger amount of Aβ_{42} fibrillation formation. However, the fluorescence intensity of Aβ_{42} treated with gCDs significantly decrease and the inhibition efficiency is only 62.97% (Fig. 2i). gCDs-E treated group shows a weak fluorescence signal, indicating that Aβ_{42} fibrillation formation is completely suppressed, and the inhibition efficiency of gCDs-E is higher than 90%. As shown in Fig. 2j, the ThT level of Aβ_{42} aggregate samples diminished distinctively in the presence of gCDs and gCDs-E during 24 h of incubation, and the disaggregation efficiency of gCDs and gCDs-E were 65% and 76%, respectively. We also used AFM to research Aβ_{42} treated with gCDs and gCDs-E. As shown in Figure 2l, non-treated Aβ_{42} is mainly long fibrils. Aβ_{42} treated with gCDs and gCDs-E were unable to form fibrils or other aggregation. In AFM, these Aβ_{42} fibrils or clusters have average heights of ~23.7 nm, compared to heights of ~3.1 and ~1.4 nm observed for Aβ_{42} treated with gCDs and gCDs-E (Figure 2m), respectively.

According to the previous reports, hydrophobic and electrostatic

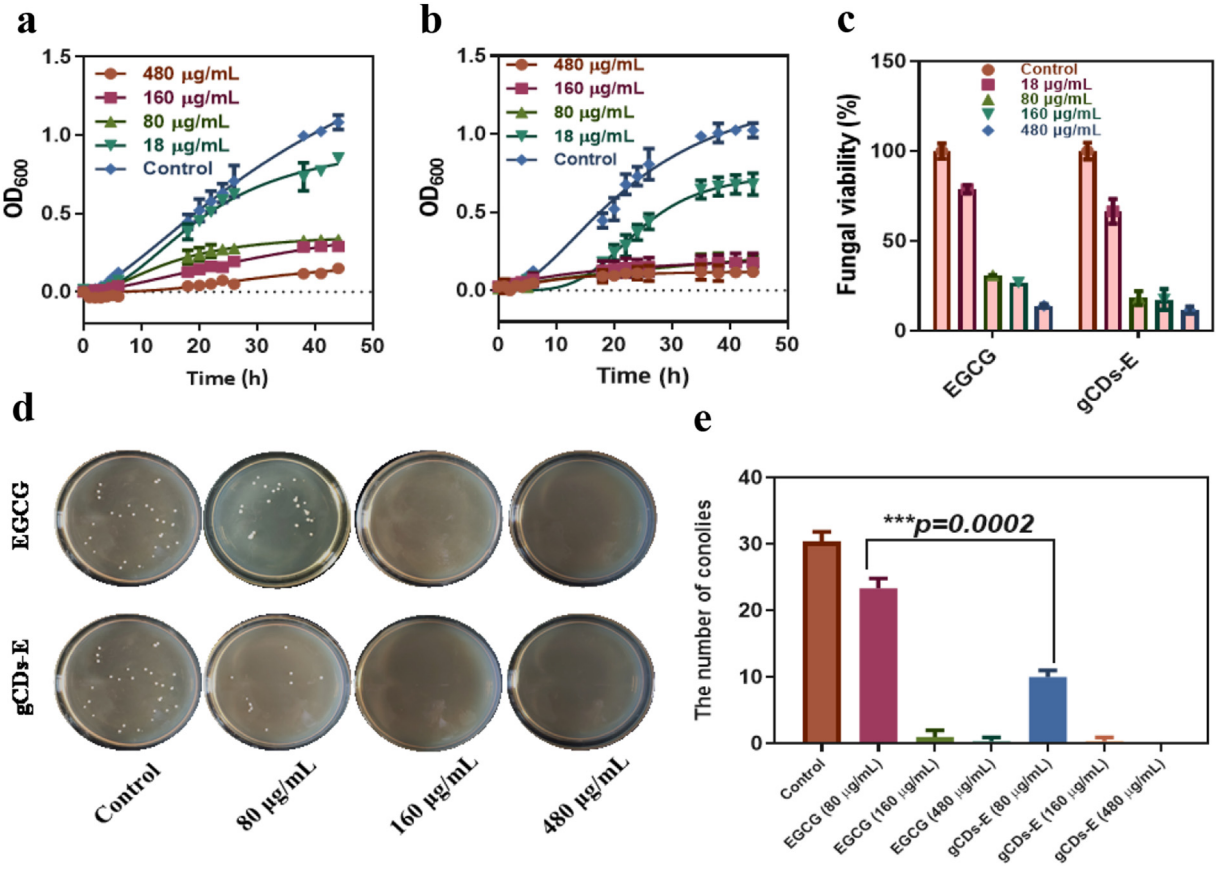

Fig. 3. (a) and (b) The growth curves of *Candida albicans* after adding EGCG or gCDs-E with different concentrations. (c) The corresponding fungi survival rates after 48 h. (d) and (e) Antifungal activities of the EGCG or gCDs-E against *Candida albicans* evaluated by a standard plate count method.

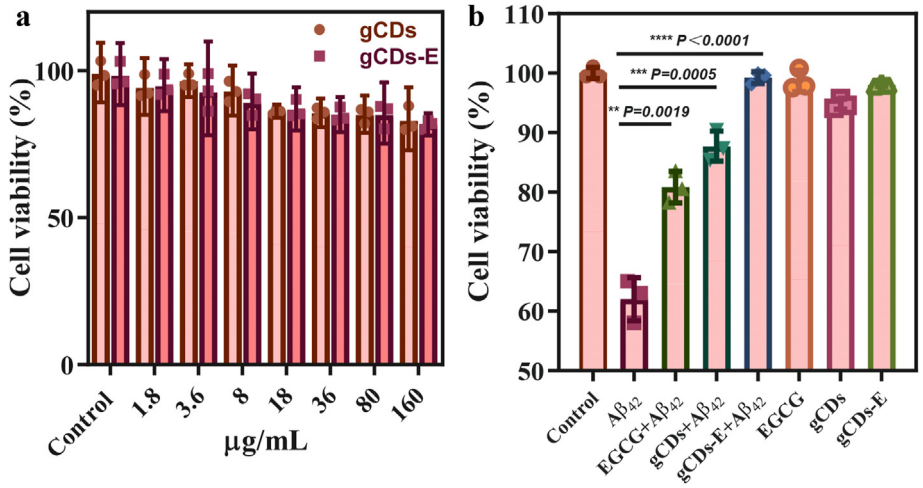

Fig. 4. (a) The dose dependent cytotoxicity of gCDs and gCDs-E towards neuron cells (SK-N-SH) as determined by CCK-8. (b) Effects of EGCG, gCDs and gCDs-E on cell viability against Aβ-mediated cytotoxicity.

interactions play important roles in the process of interaction between the carbon materials and Aβ peptides [65–68]. Previous study showed that the negative charges of nanomaterials can effectively interact with positively charged His residues of Aβ peptides [65,66]. In this work, gCDs own a similar structure with graphene, and can interact with Aβ peptide by hydrophobic interactions. Zeta potential analysis showed that the surface of gCDs and gCDs-E were both negatively charged (Fig. S10). Therefore, hydrophobic interactions and electrostatic interactions are the two most important factors of inhibiting the Aβ peptide aggregation. More importantly, EGCG can directly bind with unfolded protein and react with free primary amine groups of Aβ peptide, forming a Schiff base, and inducing fibril remodeling [69]. These mechanisms have

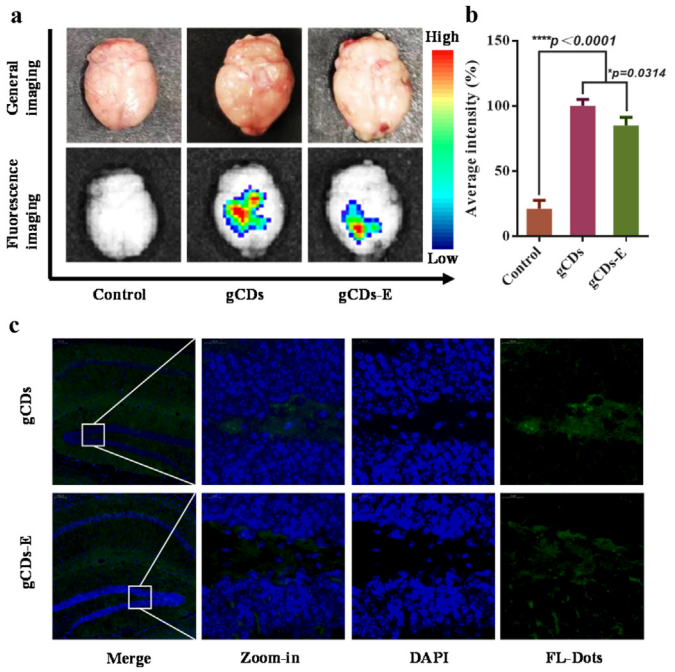

Fig. 5. (a) The photographs of representative brains of mice after the treatments and fluorescence imaging of brains after different treatments (Control: PBS solution; gCDs solution; gCDs-E solution). (b) The corresponding average fluorescence intensity. (c) CLSM images of brain tissue slices of normal mice treated by gCDs and gCDs-E (Blue and Green signals are DAPI and FL-Dots, respectively). FL-Dots include gCDs and gCDs-E.

greatly promoted the efficiency of gCDs-E to inhibit Aβ fibrillation.

2.3. Evaluation of gCDs-E for inhibiting Candida albicans

Some research reveals that blood-borne infections with *Candida albicans* are implicated in diseases as diverse as AD [32]. Here, we verify the inhibition ability of gCDs-E for *Candida albicans* and further demonstrate a novel strategy of treating AD. Fig. 3a and b shows the growth curves of *Candida albicans* incubated with EGCG and gCDs-E, respectively. The OD_{600} values of both EGCG and gCDs-E decreased sharply at 80 μg mL^{-1} within 24 h. As expected, the antifungal efficiency remarkably increased with the increasing concentration of EGCG or gCDs-E, and the fungi survival rates of *Candida albicans* treated with EGCG and gCDs-E were only 13.9% and 11.5% at 480 μg mL^{-1} after 24 h (Fig. 3c), respectively. Then, morphology changes of the *Candida albicans* were investigated by scanning electron microscopy (SEM). The *Candida albicans* incubated with gCDs-E shows serious damage in the cell wall and leakage of cellular contents comparing with EGCG treated samples (Fig. S11). However, gCD have not the antifungal properties based on the growth curves of *Candida albicans* (Fig. S12). Next, the antifungal activities of EGCG and gCDs-E were evaluated by a standard plate count method using *Candida albicans*. Remarkably, EGCG and gCDs-E displayed a concentration-dependent antifungal activity against *Candida albicans* (Fig. 3d and e). Compared with EGCG (suppression effect: 23%), an obvious suppression effect on fungal viability (67.2%) was observed for gCDs-E at a low concentration of 80 μg mL^{-1}. These results indicated that EGCG assembled with gCDs demonstrate effective antifungal functions against *Candida albicans*.

2.4. Anti-Aβ toxicity evaluation

In order to evaluate the biological response of the prepared nanomaterials, we first explored its biocompatibility by measuring cytotoxicity in the human neuroblastoma cell line SK-N-SH. SK-N-SH Cells treated with gCDs or gCDs-E for 24 h were assessed by CCK-8 assay for detecting the cell viability [25,70]. Fig. 4a shows the cytotoxicity of various concentrations of the prepared nanomaterials from 1.8 to 160 μg mL^{-1}, Cell viability is observed approximate 85% at a concentration of 160 μg mL^{-1}, which suggests that gCDs-E are almost non-toxic to SK-N-SH cells and can be utilized for further *in vitro* experiments. To measure the *anti*-Aβ toxicity of gCDs-E, gCDs and EGCG, we detected the cell viability of SK-N-SH cells treated with $A\beta_{42}$ in the absence and presence of gCDs-E, gCDs and EGCG. As shown in Fig. 4b, $A\beta_{42}$ alone exhibited obvious toxicity and cell viability was only 62%. However, gCDs-E, gCDs and EGCG were added to suppress the toxicity of $A\beta_{42}$. The gCDs-E treated groups showed remarkably higher cell viabilities than gCDs and EGCG treated groups. This difference in cell viabilities indicated that the combination of EGCG and gCDs resulted in a synergistic *anti*-Aβ-toxicity effect. In addition, gCDs-E, gCDs and EGCG alone exhibited high cell viability with approximate 100%. gCDs-E showed the highest cell viability (99.2%), close to that of the control group (100%) and was screened as the potential lead drugs for inhibiting Aβ-induced toxicity and treating AD.

2.5. Brain penetration of the gCDs-E in vivo

Blood-brain barrier (BBB), is a widely considered *in vivo* experiment as a key factor in the treatment of AD. In order to evaluate the ability of gCDs and gCDs-E for overcoming BBB, we intravenously injected a dose of 1 mg mL^{-1} samples into mice. The mice were sacrificed and the brains were harvested for fluorescence imaging. As shown in Fig. 5a, the higher fluorescence signal in gCDs indicated that this gCDs can reach to the brain compared with PBS treated group. In addition, the fluorescence signal of gCDs-E is also higher than PBS treated group, indicating that gCDs-E also can cross the BBB. The ability of gCDs and gCDs-E for overcoming BBB was further confirmed by immunohistochemical method. As shown in Fig. 5b, the distribution of the gCDs or gCDs-E in the hippocampus was further analyzed. The CLSM images displayed obvious dots of green signals (green fluorescence from gCDs; blue fluorescence from DAPI) in the gCDs and gCDs-E treated group. These results suggested that gCDs and gCDs-E could effectively overcome the BBB *in vivo*. According to previous report [11,71–73], the main method for nanomedicine to cross the BBB is to modify its surface with glucose. As outstanding candidate ligands for promoting BBB traversal, glucose, the main energy source in the brain, is notable because glucose transporter-1 (GLUT1) is expressed at a remarkably high level compared to many other receptors and transporters in brain capillary endothelial cells [74]. Based on current and previous work [75], the surface of gCDs carbonized by glucose own incompletely reacted glucose structure, which will promote the glucose-functionalized gCDs to cross the BBB through the dependence of glucose transporters.

2.6. Improvement of memory deficits of APP/PS1 mice

As shown in Fig. 6a, the Morris Water Maze test was used to detect whether gCDs or gCDs-E could improve spatial learning ability in APP/PS1 mice. As expected, non-treated APP/PS1 mice showed significant learning deficits. Fig. 6b shows that the learning ability of gCDs-E-treated mice were improved, such as a shorter escape latency after 5 days, longer residence time at the target platform position, and a greater possibility of

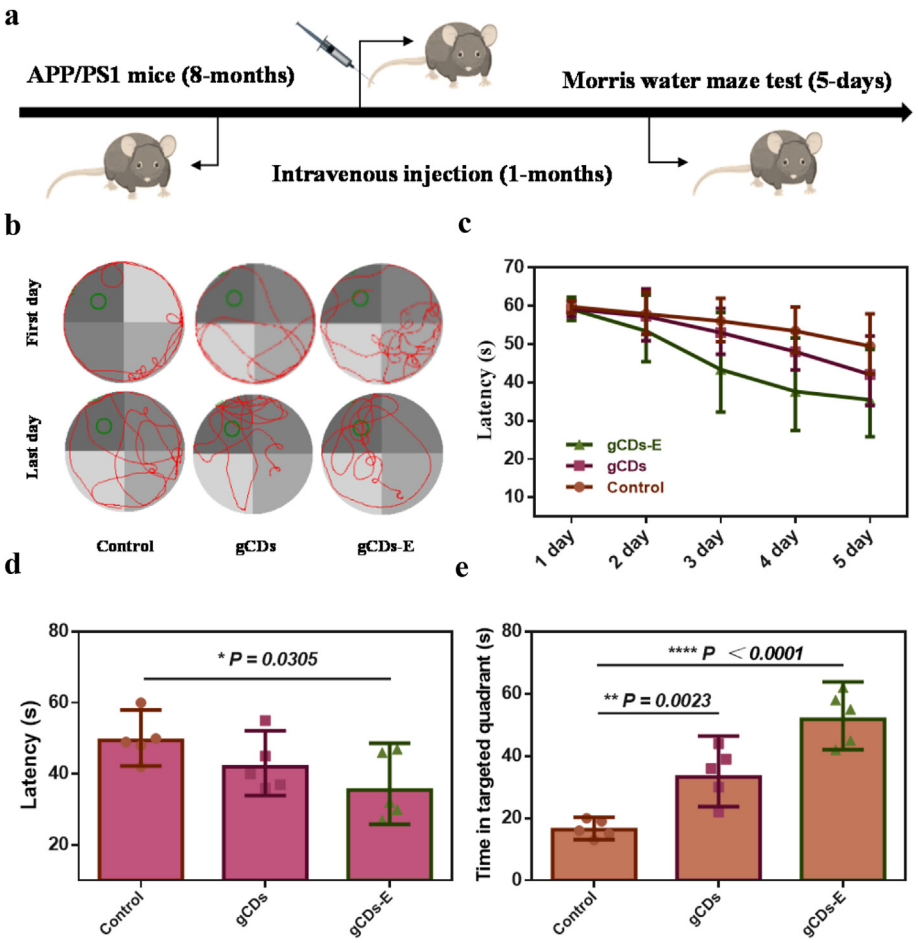

Fig. 6. (a) Time schedule of the experimental procedure for APP/PS1 mice. (b) Representative searching paths in Morris Water Maze (MWM) test. (c) Comparison of learning path delay time between different treatment groups. (d) The latency during the memory test in the MWM probe trial without a platform. (e) The percent (s) of time in the targeted quadrant where the platform had been located during the memory test in the MWM probe trial.

reaching the target platform quadrant (Fig. 6b, c and d). More importantly, gCDs-E exhibit significant performance improvement in APP/PS1 mice cognitive ability compared with that of gCDs.

In addition, key factors of AD about Aβ plaques and neuronal loss in the hippocampus were evaluated. Nissl staining analysis (Fig. 7a and c) results reveal that the non-treated and gCDs-treated APP/PS1 mice had few Nissl bodies compared to gCDs-E treated group. In other words, gCDs-E treatment added more neurons with restored integrity, and gCDs treatments is less effective than gCDs-E. An immunohistochemistry analysis was also performed on mouse brains (Fig. 7b and d). The Aβ plaques in the gCDs-E-treated APP/PS1 mice decreased significantly compared with the control and gCDs-treated AD mice, indicating that gCDs-E reduces Aβ plaques. These results indicated that gCDs-E had synergistic therapeutic effects on reducing amyloid plaque and inhibiting neuronal loss in APP/PS1 mice.

2.7. Biocompatibility evaluation of nanomaterials

The cytotoxicity is primary factor for application of nanomaterials in biomedicine. As shown in Fig. S13, the cell viability of the NRK cells remains higher than 90% when the concentration of gCDs and gCDs-E increases from 1.8 to 160 μg mL^{-1}. This result indicates that no significant toxicity was noted in either system at the tested exposure levels. Hemocompatibility is the first-level evaluation before the nanomaterials was administered via tail vein injection [20]. As shown in Fig. S14, hemolysis degree of gCDs and gCDs-E is relatively low and the value of gCDs are 2.459% (80 μg/mL) and 2.76% (160 μg/mL), and the value of gCDs-E are 2.7% (80 μg/mL) and 3.93% (160 μg/mL), respectively. These results indicate that the gCDs and gCDs-E are safe for intravenous administration. The biocompatibility of gCDs and gCDs-E was analyzed in APP/PS1 mice, and the change in body weight after injecting the drug was measured (Fig. 7e). No significant difference in body weight was observed among gCDs or gCDs-E-treated APP/PS1 mice within 17 days. Further, normal mice were treated with different treatments (including PBS, gCDs, and gCDs-E treating), and no abnormal behavior was monitored and the main organs (Heart, Liver, Spleen, Lung, Kidney) of the mice were harvested for histopathological analysis. As shown in Fig. 7f, no obvious pathological abnormalities were detected, which indicated that gCDs and gCDs-E had a favorable biocompatibility, and could be used for further application of AD treatment.

3. Conclusions

In conclusion, we successfully fabricated dual-target nanoassemblies (namely gCDs-E) assembled with EGCG and glycosylated carbon dots, and have proposed an innovative multi-target therapeutic strategy for the treatment of AD. It is demonstrated that gCDs-E can effectively prevent misfolding of Aβ and inhibit its aggregation *in vitro*, and the inhibition

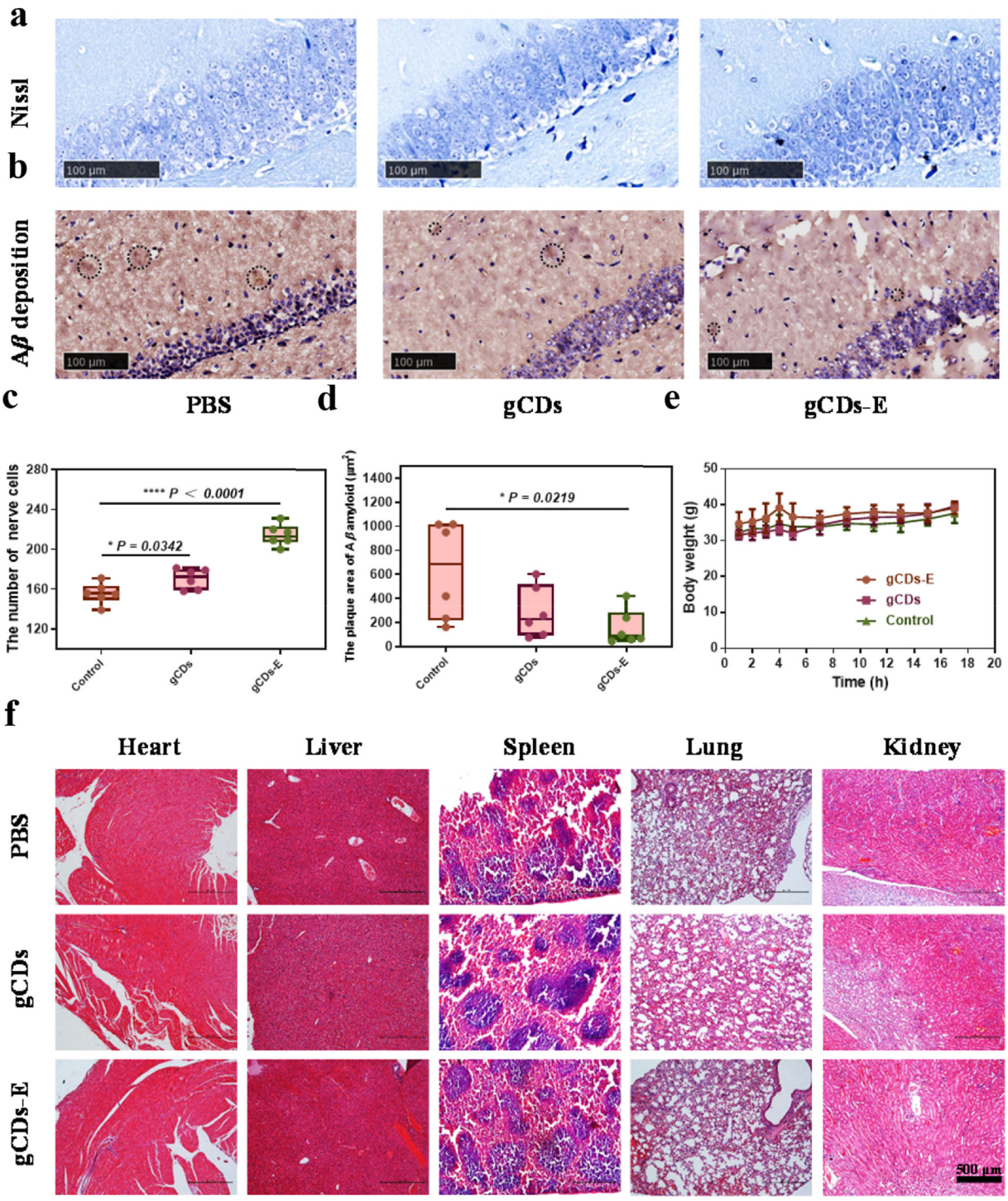

Fig. 7. (a) The Nissl staining of nerve cells in the brains of AD control mice, AD mice treated with gCDs, and AD mice treated with gCDs-E. (b) The immunohistochemical analysis of Aβ_{42} deposition in the brains of AD control mice, AD mice treated with gCDs, and AD mice treated with gCDs-E. (c) and (d) were the quantified results of (a, b), respectively. (e) Relative body weight of APP/PS1 mice after the treatment of PBS, gCDs, and gCDs-E in 17 days. (f) Hematoxylin and eosin (H&E) staining of the main organs (Heart, Liver, Spleen, Lung, Kidney) after PBS, gCDs, and gCDs-E injection.

efficiency is higher than 90%. CCK-8 experiments show that gCDs-E can remarkably reduce Aβ-mediated cytotoxicity. Importantly, gCDs-E also can suppress *Candida albicans* activity, which could prevent memory loss caused by fungal infection. *In vitro* and *in vivo* experiments confirm the gCDs-E's high-biocompatibility and ability of BBB penetration. Furthermore, the gCDs-E can greatly clean Aβ deposition and improve memory impairment in APP/PS1 transgenic AD model mice. Therefore, gCDs-E nanomaterials can serve as a novel nanoplatform, exhibiting great potential therapeutic prospect in the treatment of AD.

Credit author statement

Chaoren Yan and Chaoli Wang: Investigation, Writing-original draft, Writing-review & editing, Visualization, Formal analysis. **Yonggang Teng and Xu Shao**: Conceptualization, Formal analysis, Investigation, Writing-original draft, Writing-review & editing. **Qi Shu**: Methodology, Software, Writing-review & editing. **Ping Guan**: Formal analysis, Writing-original draft. **Chaoli Wang**: Resources, Software, Formal analysis. **Xiaoling Hu, Ping Guan and Yuan Cheng**: Supervision, Conceptualization, Resources, Funding acquisition, Project administration. **Chaoli Wang and Yuan Cheng**: Methodology, Conceptualization, Writing-review & editing, Project administration.

Declaration of competing interest

The authors declare that they have no known competing financial interests or personal relationships that could have appeared to influence the work reported in this paper.

Acknowledgements

This work was supported financially by the National Natural Science Foundation of China (31771087), Innovation Capability Support Plan of Shaanxi Province (No. 2020TD-041), Shaanxi Key Research & Development Program Foundation (2020GY-285). Shaanxi Natural Science Foundation (2021JM-238), Innovation Foundation for Doctor Dissertation of Northwestern Polytechnical University (CX2021112). We thank the Analytical and Testing Center of Northwestern Polytechnical University for equipment supporting. Thanks to my girlfriend (Ms. Qu) for encouragement.

Appendix A. Supplementary data

Supplementary data to this article can be found online at https://doi.org/10.1016/j.mtbio.2021.100167.

References

[1] K. Blennow, M. Leon, H. Zetterberg, Alzheimer's disease, Lancet 368 (2006) 387–403.
[2] M.P. Mattson, Pathways towards and away from Alzheimer's disease, Nature 430 (2016) 631–639.
[3] J. Sevigny, P. Chiao, T.P.H. Weinreb, L. Williams, M. Maier, R. Dunstan, S. Salloway, T. Chen, Y. Ling, J. Gorman, F. Qian, M. Arastu, M. Li, S. Chollate, M. Brennan, O. Quintero, R.H. Scannevin, The antibody aducanumab reduces Aβ plaques in Alzheimer's disease, Nature 537 (2016) 50–56.
[4] K. Fuyuki, H. Masato, Reconsideration of amyloid hypothesis and tau hypothesis in alzheimer's disease, Front. Neurosci. 12 (2018) 25.
[5] C.A. Lemere, E. Masliah, Can Alzheimer disease be prevented by amyloid-β immunotherapy, Nat. Rev. Neurol. 6 (2010) 108–119.
[6] M. Arbel, B. Solomon, Immunotherapy for Alzheimer's disease: attacking amyloid-β from the inside, Trends Immunol. 28 (2007) 511–513.
[7] C.H.V. Dyck, Anti-amyloid-β monoclonal antibodies for Alzheimer's disease: Pitfalls and Promise, Biol. Psychiatry 83 (2018) 311–319.
[8] S. Lesne, M.T. Koh, L. Kotilinek, R. Kayed, C.G. Glabe, A. Yang, M. Gallagher, K.H. Ashe, A specific amyloid-β protein assembly in the brain impairs memory, Nature 440 (2006) 352–357.
[9] J. Shin, P. Verwilst, H. Choi, S. Kang, J. Han, N.H. Kim, J.G. Choi, M.S. Oh, J.S. Hwang, D. Kim, I.M. Jung, J. Kim, Harnessing intramolecular rotation to enhance two-photon imaging of Aβ plaques through minimizing background fluorescence, Angew. Chem. 131 (2019) 5704–5708.
[10] R. Zhang, Y. Li, B. Hu, Z. Lu, J. Zhang, X. Zhang, Traceable nanoparticle delivery of small interfering RNA and retinoic acid with temporally release ability to control neural stem cell differentiation for alzheimer's disease therapy, Adv. Mater. Catal. 28 (2016) 6345–6352.
[11] J. Xie, D. Gonzalez-Carter, T.A. Tockary, N. Nakamura, Y. Xue, M. Nakakido, H. Akiba, A. Dirisala, X. Liu, K. Toh, T. Yang, Z. Wang, S. Fukushima, J. Li, S. Quader, K. Tsumoto, T. Yokota, Y. Anraku, K. Kataoka, Dual-sensitive nanomicelles enhancing systemic delivery of therapeutically active antibodies specifically into the brain, ACS Nano 14 (2020) 6729–6742.
[12] Y. Pan, H. Wang, X. Xu, H. Tian, X. Xu, Coassembly of macrocyclic amphiphiles for anti-β-amyloid therapy of Alzheimer's disease, CCS Chem 2 (2020) 2485–2497.
[13] H. Yang, X. Li, L. Zhu, X. Wu, S. Zhang, F. Huang, X. Feng, L. Shi, Heat shock protein inspired nanochaperones restore amyloid-β homeostasis for preventative therapy of alzheimer's disease, Adv. Sci. 6 (2019) 1901844.
[14] R. Liu, J. Yang, L. Liu, Z. Lu, X. Zhang, An "amyloid-β cleaner" for the treatment of alzheimer's disease by normalizing microglial dysfunction, Adv. Sci. 7 (2020) 1901555.
[15] Y. Chung, C.H. Lee, J. Lim, J. Jang, H. Kang, C.B. Park, Photomodulating carbon dots for spatiotemporal suppression of alzheimer's β-amyloid aggregation, ACS Nano 14 (2020) 16973–16983.
[16] M. Ma, Z. Liu, N. Gao, X. Qu, Self-protecting biomimetic nanozyme for selective and synergistic clearance of peripheral amyloid-β in an Alzheimer's disease model, J. Chem. Soc. 142 (2020) 21702–21711.
[17] Z. Du, M. Li, J. Ren, Current strategies for modulating Aβ aggregation with multifunctional agents, Acc. Chem. Res. 54 (2021) 2172–2184.
[18] D. Pisa, R. Alonso, A. Juarranz, A. Rábano, L.J. Carrasco, Direct visualization of fungal infection in brains from patients with alzheimer's disease, Alzheimer's Dis. 43 (2015) 613–624.
[19] S.S. Dominy, C. Lynch, F. Ermini, M. Benedyk, A. Marczyk, A. Konradi, M. Nguyen, U. Haditsch, D. Raha, C. Griffin, L.J. Holsinger, S. Arastu-Kapur, S. Kaba, A. Lee, M.I. Ryder, B. Potempa, P. Mydel, A. Hellvard, K. Adamowicz, H. Hasturk, G.D. Walker, E.C. Reynolds, R.L.M. Faull, M.A. Curtis, M. Dragunow, J. Potempa, Porphyromonas gingivalis in Alzheimer's disease brains: evidence for disease causation and treatment with small-molecule inhibitors, Sci. Adv. 5 (2019) eaau3333.
[20] Y. Wu, S. Du, J.L. Johnson, H. Tung, C.T. Landers, Y. Liu, B.G. Seman, R.T. Wheeler, M. Costa-Mattioli, F. Kheradmand, D.B. Zheng Corry, Microglia and amyloid precursor protein coordinate control of transient Candida cerebritis with memory deficits, Nat. Commun. 10 (2019) 58.
[21] D.K.V. Kumar, S.H. Choi, K.J. Washicosky, W.A. Eimer, S. Tucker, J. Ghofrani, A. Lefkowitz, G. McColl, L.E. Goldstein, R.E. Tanzi, R.D. Moir, Amyloid-β peptide protects against microbial infection in mouse and worm models of Alzheimer's disease, Sci. Transl. Med. 8 (2016), 340ra72.
[22] A. Ruth, P. Diana, M.A. Isabel, M. Esperanza, R. Alberto, C. Luis, Fungal infection in patients with alzheimer's disease, J. Alzheim. Dis. 41 (2014) 301–311.
[23] P. Velander, L. Wu, F. Henderson, S. Zhang, D. Bevan, B. Xu, Natural product-based amyloid inhibitors, Biochem. Pharmacol. 139 (2017) 40–45.
[24] L. Jia, W. Wang, Y. Yan, R. Hu, F. Liu, General aggregation-induced emission probes for amyloid inhibitors with dual inhibition capacity against amyloid β-protein and α-synuclein, ACS Appl. Mater. Interfaces 12 (2020) 31182–31194.
[25] A.N. Khan, K. Gadhave, M. Furkan, P. Kumar, R.H. Khan, Anti-tuberculotic thionamide antibiotics show antioxidative and neuronal cytoprotective nature by inhibiting amyloid formation in human insulin and amyloid β-42, J. Mol. Liq. 326 (2021) 115396.
[26] R. Ahmed, B. Vanschouwen, N. Jafari, X. Ni, J. Ortega, G. Melacini, Molecular mechanism for the (−)-Epigallocatechin gallate-induced toxic to nontoxic remodeling of Aβ oligomers, J. Am. Chem. Soc. 139 (2017) 13720–13734.
[27] S. Xiao, D. Zhou, P. Luan, B. Gu, L. Feng, S. Fan, W. Liao, W. Fang, L. Yang, E. Tao, Graphene quantum dots conjugated neuroprotective peptide improve learning and memory capability, Biomaterials 106 (2016) 98–110.
[28] K. Debnath, S. Shekhar, V. Kumar, V.N.R. Jana, Efficient inhibition of protein aggregation, disintegration of aggregates, and lowering of cytotoxicity by green tea polyphenol-based self-assembled polymer nanoparticles, ACS Appl. Mater. Interfaces 8 (2016) 20309–20318.
[29] C. Yan, N. Zhan, P. Guan, P. Chen, S. Ding, T. Hou, X. Hu, J. Wang, C. Wang, Drug-based magnetic imprinted nanoparticles: enhanced lysozyme amyloid fibrils cleansing and anti-amyloid fibrils toxicity, Int. J. Biol. Macromol. 153 (2020) 723–735.
[30] D. Huang, Y. Cao, X. Yang, Y. Liu, Q. Wang, A nanoformulation-mediated multifunctional stem cell therapy with improved beta-amyloid clearance and neural regeneration for alzheimer's disease, Adv. Mater. 33 (2021) 2006357.
[31] H. Niu, X. Hou, Y. Zhang, X. Wu, F. Deng, F. Huang, L. Shi, R. Ma, Self-assembled nanochaperones inhibit the aggregation of human islet amyloid polypeptide associated with type 2 diabetes, ACS Macro Lett. 10 (2021) 662–670.
[32] J. Sun, C. Wei, Y. Liu, W. Xie, M. Xu, H. Zhou, J. Liu, Progressive release of mesoporous nano-selenium delivery system for the multi-channel synergistic treatment of Alzheimer's disease, Biomaterials 197 (2019) 417–431.
[33] W. Wen, P. Kuo, C. Chiang, Y. Chin, M. Fu, E. Fu, Epigallocatechin-3-Gallate attenuates porphyromonas gingivalis lipopolysaccharide-enhanced matrix metalloproteinase-1 production through inhibition of interleukin-6 in gingival fibroblasts, J. Periodontol. 85 (2014) 868–875.
[34] I. Jung, D. Lee, J. Yun, A. Cho, C. Kim, Y. You, S. Kim, S. Choi, Anti-inflammatory effect of (-)-epigallocatechin-3-gallate on Porphyromonas gingivalis lipopolysaccharide-stimulated fibroblasts and stem cells derived from human periodontal ligament, J. Periodontal Implant Sci. 42 (2012) 185–195.
[35] Y. Ning, J. Ling, C. Wu, Synergistic effects of tea catechin epigallocatechin gallate and antimycotics against oral Candida species, Arch. Oral Biol. 60 (2015) 1565–1570.
[36] M. Hirasawa, K. Takada, J. Antimicrob, Multiple effects of green tea catechin on the antifungal activity of antimycotics against Candida albicans, Chemother 53 (2004) 225–229.
[37] K. Du, M. Liu, X. Zhong, W. Yao, Q. Xiao, Q. Wen, B. Yang, M. Wei, Epigallocatechin gallate reduces amyloid β-induced neurotoxicity via inhibiting endoplasmic reticulum stress-mediated apoptosis, Mol. Nutr. Food Res. 62 (2018), e1700890.
[38] J. Bieschke, J. Russ, R.P. Friedrich, D.E. Ehrnhoefer, H. Wobst, K. Neugebauer, E.E. Wanker, EGCG remodels mature α-synuclein and amyloid-β fibrils and reduces cellular toxicity, Proc. Natl. Acad. Sci. Unit. States Am. 107 (2010) 7710–7715.

[39] X. Chen, B. Liu, R. Tong, S. Ding, Jian Wu, Q. Lei, W. Fang, Improved stability and targeted cytotoxicity of epigallocatechin-3-gallate palmitate for anticancer therapy, Langmuir 37 (2021) 969–977.
[40] T. Yin, W. Xie, J. Sun, L. Yang, J. Liu, Penetratin peptide-functionalized gold nanostars: enhanced BBB permeability and NIR photothermal treatment of Alzheimer's disease using ultralow irradiance, ACS Appl. Mater. Interfaces 8 (2016) 19291–19302.
[41] M. Jeon, K. Kim, E. Kim, S. Lee, D. Kim, Emerging pathogenic role of peripheral blood factors following BBB disruption in neurodegenerative disease, Ageing Res. Rev. 68 (2021) 101333.
[42] S. Ding, A. Khan, X. Cai, Y. Song, Z. Lyu, D. Du, P. Dutta, Y. Lin, Overcoming blood–brain barrier transport: advances in nanoparticle-based drug delivery strategies, Mater. Today 37 (2020) 112–125.
[43] Z. Zhang, G. Han, J. Zhao, R. Zhang, X. Tian, Z. Liu, A. Wang, R. Liu, B. Liu, M. Han, Membrane-penetrating carbon quantum dots for imaging nucleic acid structures in live organisms, Angew. Chem. Int. Ed. 58 (2019) 7087–7091.
[44] X. Wei, L. Li, J. Liu, L. Yu, H. Li, F. Cheng, X. Yi, J. He, B. Li, Green synthesis of fluorescent carbon dots from gynostemma for bioimaging and antioxidant in zebrafish, ACS Appl. Mater. Interfaces 11 (2019) 9832–9840.
[45] F. Li, S. Li, X. Guo, Y. Dong, D. Yang, Chiral carbon dots mimicking topoisomerase I to mediate the topological rearrangement of supercoiled DNA enantioselectively, Angew. Chem. Int. Ed. 59 (2020) 11087–11092.
[46] C. Yan, L. Guo, X. Shao, Q. Shu, P. Guan, J. Wang, X. Hu, C. Wang, Amino acid–functionalized carbon quantum dots for selective detection of Al^{3+} ions and fluorescence imaging in living cells, Anal. Bioanal. Chem. 5 (2021) 3965–3974.
[47] C. Yan, C. Wang, T. Hou, P. Guan, Y. Qiao, L. Guo, Y. Teng, X. Hu, H. Wu, Lasting tracking and rapid discrimination of live gram-positive bacteria by peptidoglycan-targeting carbon quantum dots, ACS Appl. Mater. Interfaces 13 (2021) 1277–1287.
[48] Y. Liu, L. Xu, W. Dai, Ha Dong, Y. Wen, X. Zhang, Graphene quantum dots for the inhibition of β amyloid aggregation, Nanoscale 7 (2015) 19060–19065.
[49] P.Y. Liyanage, Y. Zhou, A. Alyoubi, A.S. Bashammakh, R.M. Leblanc, Pediatric glioblastoma target-specific efficient delivery of gemcitabine across the blood-brain barrier via carbon nitride dots, Nanoscale 12 (2020) 7927–7938.
[50] X. Han, J. Park, W. Wu, A. Malagon, L. Wang, R.M. Leblanc, A resorcinarene for inhibition of Aβ fibrillation, Chem. Sci. 8 (2017) 2003–3009.
[51] X. Han, Z. Jing, R.M. Leblanc, Biocompatible and blood–brain barrier permeable carbon dots for inhibition of Aβ fibrillation and toxicity BACE1 activity, Nanoscale 9 (2017) 12862–12866.
[52] E.S. Seven, Y.B. Seven, Y. Zhou, R.M. Leblanc, Crossing the blood–brain barrier with carbon dots: uptake mechanism and in vivo cargo delivery, Nanoscale Adv. 3 (2021) 3942–3953.
[53] Y. Zhou, P.Y. Liyanage, D. Devadoss, R.M. Leblanc, Nontoxic amphiphilic carbon dots as promising drug nanocarriers across the blood–brain barrier and inhibitors of β-amyloid, Nanoscale 11 (2019) 22387–22397.
[54] C. Zhao, X. Song, Y. Liu, J. Liu, Synthesis of graphene quantum dots and their applications in drug delivery, J. Nanobiotechnol. 18 (2020) 142.
[55] F. Yuan, T. Yuan, L. Sui, Z. Wang, Z. Xi, Y. Li, X. Li, L. Fan, Z. Tan, Engineering triangular carbon quantum dots with unprecedented narrow bandwidth emission for multicolored LEDs, Nat. Commun. 9 (2018) 2249.
[56] H. Yang, Y. Liu, Z. Guo, B. Lei, J. Zhuang, Hydrophobic carbon dots with blue dispersed emission and red aggregation-induced emission, Nat. Commun. 10 (2019) 1789.
[57] J. Liu, Y. Geng, D. Li, H. Yao, Z. Huo, Y. Li, K. Zhang, S. Zhu, H. Wei, W. Xu, J. Jiang, B. Yang, Deep red emissive carbonized polymer dots with unprecedented narrow full width at half maximum, Adv. Mater. (2020) 1906641.
[58] L. Wang, W. Li, L. Yin, Y. Liu, H. Guo, J. Lai, Y. Han, G. Li, M. Li, J. Zhang, R. Vajtai, P.M. Ajayan, M. Wu, Full-color fluorescent carbon quantum dots, Sci. Adv. 6 (2020), eabb6772.
[59] S. Pandit, P. Behera, J. Sahoo, M. De, In situ synthesis of amino acid functionalized carbon dots with tunable properties and their biological applications, ACS Appl. Bio Mater. 2 (2019) 3393–3403.
[60] L. Guo, H. Yan, L. Yan, L. Bai, S. Niu, Y. Zhao, A hyperbranched polysiloxane containing carbon dots with near white light emission, Polym. Chem. 12 (2021) 3582–3591.
[61] L. Bai, H. Yan, Y. Feng, W. Feng, L. Yuan, Multi-excitation and single color emission carbon dots doped with silicon and nitrogen: synthesis, emission mechanism, Fe^{3+} probe and cell imaging, Chem. Eng. J. 373 (2019) 963–972.
[62] C. Shang, N. Wei, H. Zhuo, Y. Shao, Q. Zhang, Z. Zhang, H. Wang, Highly emissive poly(maleic anhydride-alt-vinyl pyrrolidone) with molecular weight-dependent and excitation-dependent fluorescence, J. Mater. Chem. C 5 (2017) 8082–8090.
[63] J. Yang, G. Gao, X. Zhang, Y. Ma, X. Chen, F. Wu, One-step synthesis of carbon dots with bacterial contact-enhanced fluorescence emission: fast Gram-type identification and selective Gram-positive bacterial inactivation, Carbon 146 (2019) 827–839.
[64] S.N. Baker, G.A. Baker, Luminescent carbon nanodots: emergent nanolights, Angew. Chem. Int. Ed. 49 (2010) 6726–6744.
[65] I. Ahmada, A. Mozhi, L. Yang, Q. Hana, X. Liang, C. Li, R. Yang, C. Wang, Graphene oxide-iron oxide nanocomposite as an inhibitor of Aβ42 amyloid peptide aggregation Colloids, Surfnet Bull. 159 (2017) 540–545.
[66] M. Mahmoudi, F.P. Quinlan, M.P. Monopoli, Influence of the physiochemical properties of superparamagnetic iron oxide nanoparticles on amyloid β protein fibrillation in solution, ACS Chem. Neurosci. 4 (2013) 475–485.
[67] N. Zhang, X. Hu, P. Guan, K. Zeng, Y. Cheng, Adsorption mechanism of amyloid fibrils to graphene nanosheets and their structural destruction, J. Phys. Chem. C 123 (2019) 897–906.
[68] N. Zhang, J. Yeo, Y. Lim, P. Guan, K. Zeng, X. Hu, Y. Cheng, Tuning the structure of monomeric amyloid beta peptide by curvature of carbon nanotubes, Carbon 153 (2019) 717–724.
[69] F.L. Palhano, J. Lee, N.P. Grimster, J.W. Kelly, Toward the molecular mechanism(s) by which EGCG treatment remodels mature amyloid fibrils, J. Am. Chem. Soc. 135 (2013) 7503–7510.
[70] C. Wang, P. Chen, Y. Qiao, Y. Kang, C. Yan, Z. Yu, J. Wang, X. He, H. Wu, pH responsive superporogen combined with PDT based on poly Ce6 ionic liquid grafted on SiO_2 for combating MRSA biofilm infection, Theranostics 10 (2020) 4795–4808.
[71] Y. Zhou, Z. Peng, E.S. Seven, R.M. Leblanc, Crossing the blood-brain barrier with nanoparticles, J. Contr. Release 270 (2018) 290–303.
[72] Y. Anraku, H. Kuwahara, T. Yokota, K. Kataoka, Glycaemic control boosts glucosylated nanocarrier crossing the BBB into the brain, Nat. Commun. 8 (2017) 1001.
[73] S. Zhou, Q. Zhong, Y. Wang, Chemically engineered mesoporous silica nanoparticles-based intelligent delivery systems for theranostic applications in multiple cancerous/non-cancerous diseases, Coord. Chem. Rev. 452 (2022) 214309.
[74] Y. Uchida, S. Ohtsuki, Y. Katsukura, C. Ikeda, T. Suzuki, J. Kamiie, T. Terasaki, Quantitative targeted absolute proteomics of human blood–brain barrier transporters and receptors, J. Neurochem. 117 (2011) 333–345.
[75] C. Yan, X. Hu, P. Guan, Highly biocompatible graphene quantum dots: green synthesis, toxicity comparison and fluorescence imaging, J. Mater. Sci. 55 (2020) 1198–1215.